

New Li Ion Conductors and Solid State Hydrogen Storage Materials: $\text{LiM}(\text{BH}_4)_3\text{Cl}$, $M = \text{La, Gd}$

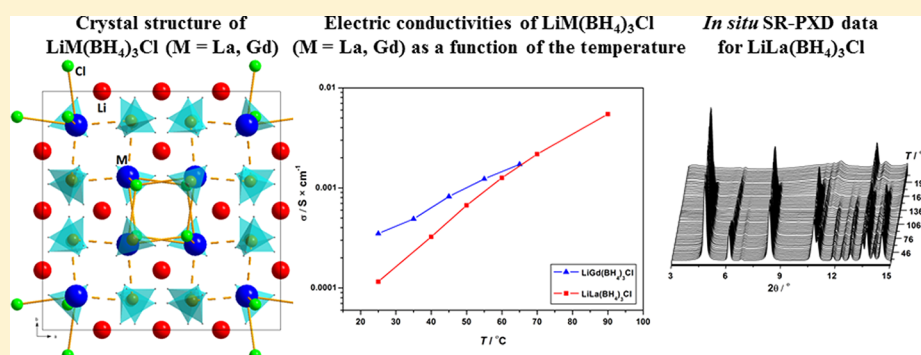
Morten B. Ley,[†] Sylvain Boulineau,[‡] Raphaël Janot,[‡] Yaroslav Filinchuk,[§] and Torben R. Jensen^{*,†}

[†]Center for Materials Crystallography (CMC), Interdisciplinary Nanoscience Center (iNANO) and Department of Chemistry, University of Aarhus, Langelandsgade 140, DK-8000 Århus C, Denmark

[‡]Laboratoire de Réactivité et Chimie des Solides, UMR 7314 CNRS, Université de Picardie - Jules Verne, Amiens Cedex, France

[§]Institute of Condensed Matter and Nanosciences, Université Catholique de Louvain, Place L. Pasteur 1, B-1348, Louvain-la-Neuve, Belgium

S Supporting Information



ABSTRACT: Multiple reaction mixtures with different composition ratios of $\text{MCl}_3\text{-LiBH}_4$ ($M = \text{La, Gd}$) were studied by mechano-chemical synthesis, yielding two new bimetallic borohydride chlorides, $\text{LiM}(\text{BH}_4)_3\text{Cl}$ ($M = \text{La, Gd}$). The Gd-containing phase was obtained only after annealing the ball-milled mixture. Additionally, a solvent extracted sample of $\text{Gd}(\text{BH}_4)_3$ was studied to gain insight into the transformation from $\text{Gd}(\text{BH}_4)_3$ to $\text{LiGd}(\text{BH}_4)_3\text{Cl}$. The novel compounds were investigated using in situ synchrotron radiation powder X-ray diffraction, thermal analysis combined with mass spectroscopy, Sieverts measurements, Fourier transform infrared spectroscopy, and electrochemical impedance spectroscopy. The two new compounds, $\text{LiLa}(\text{BH}_4)_3\text{Cl}$ and $\text{LiGd}(\text{BH}_4)_3\text{Cl}$, have high lithium ion conductivities of 2.3×10^{-4} and $3.5 \times 10^{-4} \text{ S} \cdot \text{cm}^{-1}$ ($T = 20^\circ\text{C}$) and high hydrogen densities of $\rho_m = 5.36$ and $4.95 \text{ wt } \% \text{ H}_2$, and both compounds crystallize in the cubic crystal system (space group $I-43m$) with unit cell parameter $a = 11.7955(1)$ and $a = 11.5627(1) \text{ \AA}$, respectively. The structures contain isolated tetranuclear anionic clusters $[\text{M}_4\text{Cl}_4(\text{BH}_4)_{12}]^{4-}$ with distorted cubane M_4Cl_4 cores $M = \text{La}$ or Gd . Each lanthanide atom coordinates three chloride ions and three borohydride groups, thus completing the coordination environment to an octahedron. The Li^+ ions are disordered on $2/3$ of the $12d$ Wyckoff site, which agrees well with the very high lithium ion conductivities. The conductivity is purely ionic, as electronic conductivities were measured to only 1.4×10^{-8} and $9 \times 10^{-8} \text{ S} \cdot \text{cm}^{-1}$ at $T = 20^\circ\text{C}$ for $\text{LiLa}(\text{BH}_4)_3\text{Cl}$ and $\text{LiGd}(\text{BH}_4)_3\text{Cl}$, respectively. In situ synchrotron radiation powder X-ray diffraction (SR-PXD) reveals that the decomposition products at 300°C consist of $\text{LaB}_6/\text{LaH}_2$ or $\text{GdB}_4/\text{GdH}_2$ and LiCl . The size of the rare-earth metal atom is shown to be crucial for the formation and stability of the borohydride phases in $\text{MCl}_3\text{-LiBH}_4$ systems.

INTRODUCTION

Storage of renewable energy is essential to create a new sustainable energy economy.¹ Renewable energy can be stored directly as electricity in, e.g., a Li-battery or indirectly as hydrogen in a solid state metal hydride.² Batteries are rechargeable but have limited energy storage capacity. Indeed, this calls for continued intense research within the energy storage materials scientific community. This paper describes new materials that are fast Li-ion conductors and also carry significant amounts of hydrogen.

Metal borohydrides currently receive increasing interest due to their high hydrogen densities. Unfortunately, many of the

known borohydrides exhibit poor thermodynamic and kinetic properties, which hamper their utilization in technological applications.³⁻⁶ Therefore, significant focus has been on synthesis and characterization of novel bimetal borohydrides due to the somewhat tunable decomposition temperatures of these compounds.⁷⁻¹⁰ Recently, the first two binary alkali/lanthanide borohydride chlorides, $\text{NaY}(\text{BH}_4)_2\text{Cl}_2$ ¹¹ and $\text{LiCe}(\text{BH}_4)_3\text{Cl}$,^{12,13} have been described with fascinating crystal

Received: August 6, 2012

Revised: September 13, 2012

Published: September 14, 2012

structures: $\text{NaY}(\text{BH}_4)_2\text{Cl}_2$ has a polymeric pseudo-orthorhombic crystal structure and $\text{LiCe}(\text{BH}_4)_3\text{Cl}$ contains tetranuclear anionic clusters of $[\text{Ce}_4\text{Cl}_4(\text{BH}_4)_{12}]^{4-}$ with a distorted cubane Ce_4Cl_4 core known from organic crystals. Several other binary alkali/lanthanide borohydrides have also been discovered, including $\text{LiSc}(\text{BH}_4)_4$,^{14,15} $\text{NaSc}(\text{BH}_4)_4$,¹⁶ $\text{KSc}(\text{BH}_4)_4$,¹⁷ and $\text{KY}(\text{BH}_4)_4$.¹⁸ Recent studies of these compounds reveal structures built from isolated complex anions, such as $[\text{Sc}(\text{BH}_4)_4]^-$ in $\text{MSc}(\text{BH}_4)_4$ ($\text{M} = \text{Li}, \text{Na}, \text{or K}$) and $[\text{Y}(\text{BH}_4)_4]^-$ in $\text{KY}(\text{BH}_4)_4$. Several of these mixed-metal borohydrides exhibit improved thermodynamic properties; e.g., $\text{LiSc}(\text{BH}_4)_4$ and $\text{LiCe}(\text{BH}_4)_3\text{Cl}$ are found to decompose in the temperature ranges 140–260 °C and 230–250 °C, respectively. These are significantly lower temperatures as compared to the corresponding alkali borohydrides, LiBH_4 and NaBH_4 , which decompose at approximately 380 and 400 °C, respectively.¹⁹

The complex borohydride ion may resemble the halide ions in the solid state, which might facilitate anion substitution in metal borohydrides. The halide stabilized lithium borohydrides $\text{LiBH}_4\text{--LiX}$ ($\text{X} = \text{Cl}, \text{Br}, \text{or I}$) form solid solutions, $\text{Li}(\text{BH}_4)_{1-x}\text{X}_x$, which tend to stabilize the hexagonal polymorph to room temperature.^{20–23} The hexagonal halide stabilized polymorphs $h\text{-Li}(\text{BH}_4)_{1-x}\text{X}_x$ were found to have high lithium ion conductivities in the range 10^{-5} to 10^{-4} $\text{S}\cdot\text{cm}^{-1}$ at room temperature (RT), which increase to approximately 10^{-2} $\text{S}\cdot\text{cm}^{-1}$ at 150 °C.^{24–26} The crystal structure of $\text{LiCe}(\text{BH}_4)_3\text{Cl}$ concurs with the observed high Li ion conductivity of 1.0×10^{-4} $\text{S}\cdot\text{cm}^{-1}$ at 20 °C as the tetranuclear anionic clusters of $[\text{Ce}_4\text{Cl}_4(\text{BH}_4)_{12}]^{4-}$ are charge balanced by disordered Li^+ ions occupying 2/3 of the available positions in the crystal lattice, allowing them to move within the structure.¹³ These materials are considered as possible electrolytes for solid state lithium batteries.²⁷

$\text{LaCl}_3\text{--LiBH}_4$ and $\text{GdCl}_3\text{--LiBH}_4$ systems have both been studied previously and reveal improved thermodynamic and kinetic properties, i.e., decompositions with evolution of mainly hydrogen gas in the temperature range 230–300 °C.^{28–30} Production of $\text{La}(\text{BH}_4)_3$ has been reported for the mixture of $\text{LaCl}_3\text{--LiBH}_4$.²⁸ However, no structural information is currently available. Ball-milling (BM) the mixture $\text{GdCl}_3\text{--LiBH}_4$ produces LiCl and $\text{Gd}(\text{BH}_4)_3$, which is isostructural to $\text{Y}(\text{BH}_4)_3$.³¹ However, upon heating to 200 °C, an unknown compound is formed.²⁹ This has prompted the present study, where we report on the synthesis, characterization, and thermal decomposition of two new lithium borohydride chloride materials, $\text{LiM}(\text{BH}_4)_3\text{Cl}$ ($\text{M} = \text{La or Gd}$), using in situ synchrotron radiation powder X-ray diffraction (SR-PXD), simultaneous thermal analysis and mass spectroscopy (DTA-TGA-MS and DSC), Sieverts measurements, Fourier transform infrared spectroscopy (FTIR), and electrochemical impedance spectroscopy (EIS).

EXPERIMENTAL SECTION

Synthesis. The different samples prepared for this study are summarized in Table 1. The title compounds, $\text{LiLa}(\text{BH}_4)_3\text{Cl}$ and $\text{LiGd}(\text{BH}_4)_3\text{Cl}$, were prepared from mixtures of $\text{LaCl}_3\text{--LiBH}_4$ and $\text{GdCl}_3\text{--LiBH}_4$ in the molar ratio 1:3 (s1 and s2). The samples were ball-milled (BM) in repeated sequences for 120 min applying 2 min BM and 2 min pauses using a Fritsch Pulverisette 4 planetary mill under inert conditions (argon atmosphere) in 80 mL tungsten carbide containers with tungsten carbide balls (o.d. 10 mm). The sample to ball mass

Table 1. Composition of the Investigated Samples and Products Obtained after BM

sample	reactants	ratio	method	products
s1	$\text{LaCl}_3\text{--LiBH}_4$	1:3	BM	$\text{LiLa}(\text{BH}_4)_3\text{Cl}$, LiCl
s2	$\text{GdCl}_3\text{--LiBH}_4$	1:3	BM	$\text{Gd}(\text{BH}_4)_3$, LiCl
s3	s2		solvent extraction	$\text{Gd}(\text{BH}_4)_3$
s4	$\text{LaCl}_3\text{--LiBH}_4$	1:3	BM/heating	$\text{LiLa}(\text{BH}_4)_3\text{Cl}$, LiCl
s5	$\text{GdCl}_3\text{--LiBH}_4$	1:3	BM/heating	$\text{LiGd}(\text{BH}_4)_3\text{Cl}$, LiCl

ratio was approximately 1:35. Speeds of the main disk and the planetary disks were 200 and 560 rpm, respectively.

A solvent-extracted sample of $\text{Gd}(\text{BH}_4)_3$ (s3) was obtained from s2 using solvent-based extraction techniques.³² Samples s4 and s5 for conductivity measurements were obtained mechano-chemically as described above. Afterward, sample s4 was annealed at 200 °C for 30 min at $p(\text{H}_2) = 10$ bar to increase the weight fraction of $\text{LiLa}(\text{BH}_4)_3\text{Cl}$. Sample s5 was then annealed at 220 °C for 45 min at $p(\text{H}_2) = 10$ bar to produce the new compound, $\text{LiGd}(\text{BH}_4)_3\text{Cl}$. Annealing was in both cases performed in a homemade autoclave connected to a gas supply system. All preparation and manipulation of the samples were performed in a glovebox with a circulation purifier maintained under an argon atmosphere with less than 1 ppm of O_2 and H_2O . The chemicals used were lanthanum chloride, LaCl_3 (Sigma-Aldrich 99.9%), gadolinium chloride, GdCl_3 (Sigma-Aldrich 99.9%), and lithium borohydride, LiBH_4 (Sigma-Aldrich, 95%). All chemicals were used as received.

Laboratory Structural Characterization. All samples were initially investigated using laboratory powder X-ray diffraction (PXD) to identify the reaction products and estimate the crystallinity of the samples. PXD measurements were performed in Debye–Scherrer transmission geometry using a Stoe diffractometer equipped with a curved $\text{Ge}(111)$ monochromator ($\text{Cu K}\alpha_1$ radiation, $\lambda = 1.54060$ Å) and a curved position-sensitive detector. Data were collected at room temperature (RT) in the 2θ -range 4 and 127°. Phase analysis of samples used for Li ion conductivity measurements and samples from the Sieverts measurements were performed using a Rigaku Smart Lab configured with a Cu source and a parallel beam multilayer mirror ($\text{Cu K}\alpha_1$ radiation, $\lambda = 1.540593$ Å, $\text{Cu K}\alpha_2$ radiation, $\lambda = 1.544414$ Å). Data were measured in the 2θ -range 5 to 70° at 2°/min. All air-sensitive samples were mounted in a glovebox in 0.5 mm glass capillaries sealed with glue.

Infrared spectra of BM samples as well as samples from the Sieverts measurement were measured using a Nicolet 380 Avatar Fourier transform infrared spectrometer (FTIR) in transmission mode. The samples were shortly exposed to air when mounted in the spectrometer.

In Situ Time-Resolved Synchrotron Radiation Powder X-ray Diffraction. In situ time-resolved synchrotron radiation powder X-ray diffraction data (SR-PXD) were collected at the Swiss-Norwegian Beamlines (SNBL) at the European Synchrotron Radiation Facility (ESRF) in Grenoble, France. A glass capillary (o.d. 0.5 mm) containing the sample was heated from RT to between 220 and 500 °C at a rate of 2 or 5 °C/min, while SR-PXD data were collected.³³ The temperature was controlled with a Cyberstar hot air blower. The data were collected during two visits at the SNBL using a MAR345 image plate detector at a sample to detector distance of 250 mm and selected X-ray wavelengths of $\lambda = 0.69736$, 0.75338, or 0.75277

Å. The capillary was oscillated by 30° during 30 s exposure of the sample to the X-ray beam.

All obtained raw images were transformed to 2D-powder patterns using the FIT2D program³⁴ and calibration measurements of the standard NIST LaB₆ sample, masking diffraction spots from the single-crystal sapphire sample holder. Uncertainties of the integrated intensities were calculated at each 2θ-point by applying Poisson statistics to the intensity data, considering the geometry of the detector.³⁵

Structural Solution of LiM(BH₄)₃Cl (M = La or Gd). SR-PXD data collected at ~115 °C for LaCl₃–LiBH₄ (1:3, s1) and at ~225 °C for GdCl₃–LiBH₄ (1:3, s2) containing the highest amount of the new compounds were selected for indexing and structure solution. The PXD patterns of both compounds have a clear resemblance to the pattern observed for LiCe(BH₄)₃Cl. Hence, structure refinement was performed in space group *I*-43*m* using atomic coordinates from LiCe(BH₄)₃Cl. The cell parameters for La and Gd compounds are $a = 11.7955(1)$ and $a = 11.5627(1)$ Å, respectively.³⁶ Lanthanum, gadolinium, and chloride atoms are located on the 8*c* Wyckoff site, and boron is located on the 24*g* Wyckoff site. The structure contains three different hydrogen positions; i.e., one hydrogen (H1) is positioned on the 48*h* site, and two (H2 and H3) are found on 24*g* Wyckoff sites. Li atoms are positioned on the 12*c* Wyckoff site. The occupancy for the Li atoms is refined to ~4 atoms per unit cell for both compounds. However, since both structures must be neutral, the idealized occupancy for Li is 2/3 corresponding to 8 Li ions per unit cell. The final refinement for LiLa(BH₄)₃Cl (Figure 1a) resulted in the following refinement factors, $R_B = 2.01%$, $R_F = 1.56%$, $R_p = 2.03%$, $R_{wp} = 2.44%$ (not corrected for background) and $R_p = 4.51%$, $R_{wp} = 4.83%$ (corrected for background), and $\chi^2 = 107$. The final refinement using the Rietveld method for LiGd(BH₄)₃Cl (Figure 1b) resulted in the refinement factors, $R_B = 2.29%$, $R_F = 1.20%$, $R_p = 2.07%$, $R_{wp} = 2.56%$ (not corrected for background) and $R_p = 5.60%$, $R_{wp} = 5.98%$ (corrected for background), and $\chi^2 = 6290$. The χ^2 values are high due to the very high counting statistics accumulated by the 2D detector. The atomic coordinates for LiLa(BH₄)₃Cl and LiGd(BH₄)₃Cl are shown in Tables S1 and S2 of the Supporting Information.

Conductivity Measurements. Electrochemical Impedance Spectroscopy (EIS) measurements were performed using a BioLogic VMP3 potentiostat-galvanostat. Steel disks, covered by carbon sheets to improve the interface with our materials, were used as electrodes. Impedance (a.c.) spectra were recorded at RT between 1 MHz and 10 mHz, with a voltage perturbation of 25 mV. Temperature-dependent measurements were also performed using a specifically developed two-electrode Swagelok cell screwed with metallic rings ensuring a perfect airtightness of the cell at temperatures up to 300 °C.

From the Nyquist plots of the complex impedance (imaginary part Z_{im} as a function of the real part Z_{re}), the resistances of the samples were obtained from the diameter of the semicircle and from the intercept on the Z_{re} axis for LiBH₄ (reference sample) and LiM(BH₄)₃Cl (M = La or Gd), respectively. The conductivity measurements were performed on pellets made from samples LaCl₃–LiBH₄ (1:3, s4) and GdCl₃–LiBH₄ (1:3, s5). The pellets with a diameter of 10 mm were prepared by using a uniaxial press (900 MPa). Sintering of the pellets was performed at RT due to the possible decomposition of the materials at elevated temperatures. The pellet densities were ca. 1.58 and 1.89 g·cm⁻³, which correspond to a compactness of 85–88%, calculated using

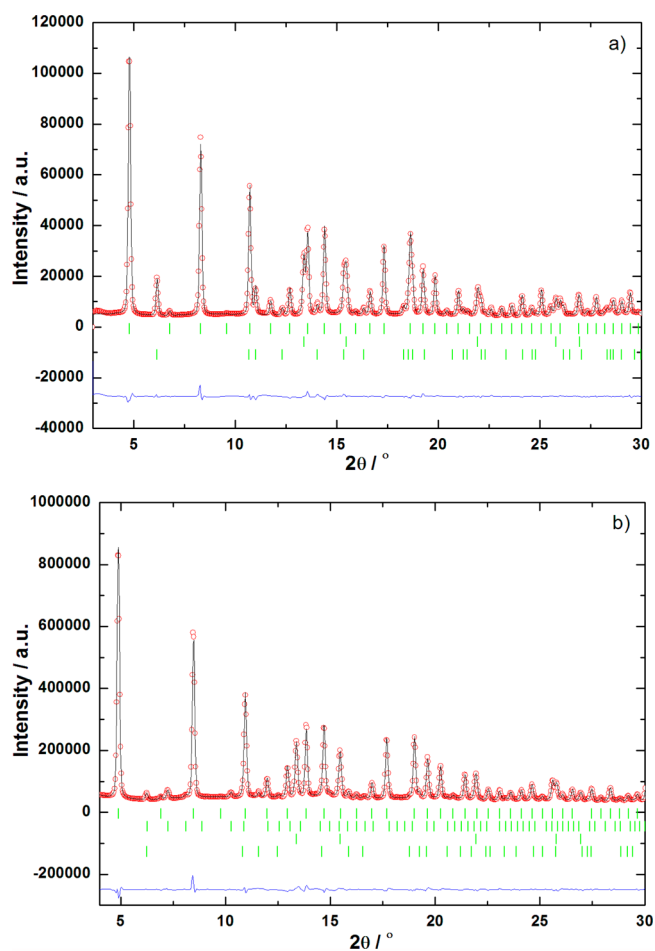


Figure 1. Rietveld refinement of SR-PXD data for (a) LaCl₃–LiBH₄ (1:3, s1) data measured at $T \sim 115$ °C and (b) GdCl₃–LiBH₄ (1:3, s2) data measured at $T \sim 225$ °C. Tic marks (a) LiLa(BH₄)₃Cl (top), unreacted LaCl₃ (bottom), and LiCl (middle). Tic marks (b) LiGd(BH₄)₃Cl (top), Gd(BH₄)₃ (2. from the top), LiCl (3. from the top), and unreacted GdCl₃ (bottom), $\lambda = 0.69736$ Å.

the crystallographic sample densities, $\rho(\text{s4}) = 1.86$ and $\rho(\text{s5}) = 2.16$ g·cm⁻³; the latter are obtained from Rietveld refinements (see Supporting Information, Figures S1 and S2).

To demonstrate that the electric conductivities of our samples were purely ionic, electronic conductivities (e.g., only electrons as charge carriers) were measured by applying direct currents on the LiM(BH₄)₃Cl (M = La or Gd) pellets, using the same BioLogic VMP3 potentiostat-galvanostat. Successive voltage steps were applied, and for each of them, a relaxation time of 6 h was taken before measuring the current. The sensitivity of the used potentiostat is ca. 0.1 nA. From Ohm's law (e.g., plotting the voltage as a function of the current), ohmic resistances were determined, and the electronic conductivities were calculated.

Thermal Analysis and Sieverts Measurements. Samples s4 and s5 were studied by simultaneous thermogravimetric analysis (TGA), differential thermal analysis (DTA), and mass spectrometry (MS) using a Netzsch STA449C connected to a Netzsch QMS403C mass spectrometer equipped with Channeltron detector capable of multi ion detection. The transfer line was heated at 300 °C. Samples were loaded in Al₂O₃ crucibles and heated from RT to 500 °C ($\Delta T/\Delta t = 10$ °C/min) under Ar flow (50 mL/min). Differential scanning calorimetry (DSC) was also performed using a Netzsch DSC

204 F1. Samples were loaded in Al crucibles, which were sealed in the glovebox. Just before the experiment, holes were made in the crucible lids to allow gas release. Samples were heated from RT to 500 °C ($\Delta T/\Delta t = 10$ °C/min) under Ar flow (200 mL/min).

The hydrogen release and uptake of $\text{LaCl}_3\text{-LiBH}_4$ (1:3, **s1**), $\text{GdCl}_3\text{-LiBH}_4$ (1:3, **s2**), and solvent-extracted $\text{Gd}(\text{BH}_4)_3$ (**s3**) were studied using Sieverts measurements in a PCTPro 2000 apparatus.^{37,38} One desorption and one absorption cycle were measured for ca. 100 mg of material. Hydrogen desorption data were collected during heating from RT to 450 °C ($\Delta T/\Delta t = 2$ °C/min) and then keeping the temperature constant at 450 °C for 1 h with a back pressure of $p(\text{H}_2) = 1$ bar. Hydrogen absorption measurements were performed at 400 °C and $p(\text{H}_2) = 85$ bar for 12 h. All samples were studied using FTIR and PXD following the absorption measurement.

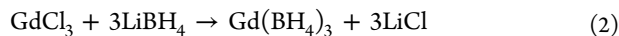
RESULTS AND DISCUSSION

Synthesis and Initial Phase Analysis. Lithium lanthanum borohydride chloride, $\text{LiLa}(\text{BH}_4)_3\text{Cl}$, was synthesized by mechano-chemistry; i.e., ball-milling $\text{LaCl}_3\text{-LiBH}_4$ (1:3, **s1**) and the SR-PXD data measured at RT shows diffraction peaks from $\text{LiLa}(\text{BH}_4)_3\text{Cl}$, LiCl , and LaCl_3 . The reaction between LaCl_3 and LiBH_4 is a complex reaction, which is believed to be a coupled metathesis and addition reaction leading to the formation of $\text{LiLa}(\text{BH}_4)_3\text{Cl}$ and LiCl according to eq 1. The optimal stoichiometry between reactants according to reaction 1 is 1:3. However, the reaction does not take place to a full extent during ball milling, as unreacted LaCl_3 is identified by PXD.



A PXD pattern measured at ~ 115 °C reveals a sample composition of $\text{LiLa}(\text{BH}_4)_3\text{Cl}$ 57 wt % (24 mol %), LiCl 33 wt % (72 mol %), and LaCl_3 10 wt % (4 mol %) (see Figure 1a). Lithium borohydride is not observed in the synthesis product by SR-PXD and may be present as an amorphous phase.¹³

Gadolinium borohydride, $\text{Gd}(\text{BH}_4)_3$, is produced by ball-milling $\text{GdCl}_3\text{-LiBH}_4$ (1:3, **s2**) according to the metathesis reaction in eq 2. Indeed, $\text{Gd}(\text{BH}_4)_3$ is isostructural to $\alpha\text{-Y}(\text{BH}_4)_3$.³¹ This reaction is also similar to that observed for the formation of $\alpha\text{-Y}(\text{BH}_4)_3$. According to the reaction scheme, the optimal ratio is again 1:3. However, as for the lanthanum system, the reaction is not complete during BM. At RT, diffraction peaks from $\text{Gd}(\text{BH}_4)_3$, GdCl_3 , and LiCl are visible, and Rietveld refinement reveals a sample composition of $\text{Gd}(\text{BH}_4)_3$ 32 wt % (18 mol %), LiCl 20 wt % (53 mol %), and GdCl_3 48 wt % (29 mol %). However, during heating at $T > 63$ °C, the reaction in eq 2 continues. At 193 °C, GdCl_3 is almost entirely consumed, and the novel compound $\text{LiGd}(\text{BH}_4)_3\text{Cl}$ begins to form by an addition reaction between $\text{Gd}(\text{BH}_4)_3$ and LiCl according to eq 3.



Rietveld analysis of the SR-PXD data collected for $\text{GdCl}_3\text{-LiBH}_4$ (1:3, **s2**) at ~ 225 °C shows an overall composition of $\text{LiGd}(\text{BH}_4)_3\text{Cl}$ 58 wt % (20.6 mol %), $\text{Gd}(\text{BH}_4)_3$ 2 wt % (0.9 mol %), LiCl 38 wt % (77.9 mol %), and GdCl_3 2 wt % (0.6 mol %) (see Figure 1b).

Crystal Structure of $\text{LiM}(\text{BH}_4)_3\text{Cl}$ (M = La, Gd). The new compounds $\text{LiLa}(\text{BH}_4)_3\text{Cl}$ and $\text{LiGd}(\text{BH}_4)_3\text{Cl}$ are isostructural

to the previously investigated compound $\text{LiCe}(\text{BH}_4)_3\text{Cl}$.¹³ Both structures contain isolated tetranuclear anionic clusters of $[\text{M}_4\text{Cl}_4(\text{BH}_4)_{12}]^{4-}$ (M = La or Gd) with a distorted cubane M_4Cl_4 core,³⁹ charge-balanced by Li^+ cations (cf. Figure 2). In

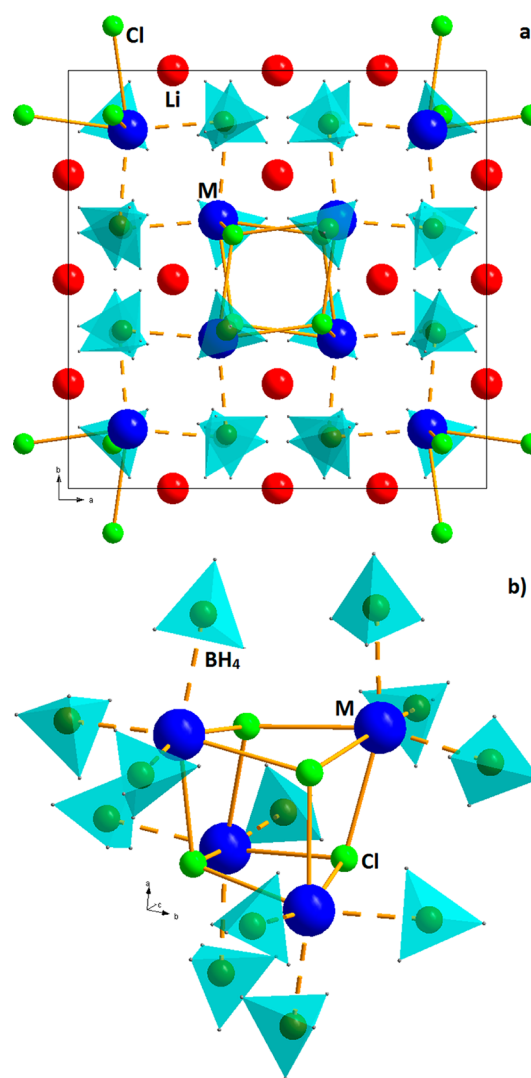


Figure 2. (a) Crystal structure of the novel compounds $\text{LiLa}(\text{BH}_4)_3\text{Cl}$ and $\text{LiGd}(\text{BH}_4)_3\text{Cl}$. The BH_4 groups are shown as light blue tetrahedra and the metals La or Gd in blue. The M–B coordinations are shown as dashed lines and M–Cl as full lines. The Li atoms (in red) are shown with full occupancy but are in fact disordered and only occupy 2/3 of the 12d Wyckoff site. (b) Isolated tetranuclear anionic clusters $[\text{M}_4\text{Cl}_4(\text{BH}_4)_{12}]^{4-}$ (M = La or Gd) with a distorted cubane M_4Cl_4 core.

$\text{LiLa}(\text{BH}_4)_3\text{Cl}$, the angles Cl–La–Cl and B–La–B are $73.1(1)^\circ$ and $99.4(5)^\circ$, respectively, and the La–Cl and La–B distances are $2.987(5)$ and $2.73(2)$ Å, respectively. In $\text{LiGd}(\text{BH}_4)_3\text{Cl}$, the angles Cl–Gd–Cl and B–Gd–B are $73.2(2)^\circ$ and $98.6(7)^\circ$, respectively. The Gd–Cl and Gd–B distances are $2.880(6)$ and $2.61(23)$ Å, respectively. Structural data are summarized in Tables S1 and S2 (Supporting Information).

During analysis of the $\text{LiLa}(\text{BH}_4)_3\text{Cl}$ and $\text{LiGd}(\text{BH}_4)_3\text{Cl}$ crystal structures, the same Li position has been adopted to the structural models as found for $\text{LiCe}(\text{BH}_4)_3\text{Cl}$. The lithium occupancy is refined to a reasonable value of $\sim 1/3$ for both title compounds (the idealized value is occupancy of 2/3 of the Li

positions to obtain charge neutrality). The lithium ion occupancy is challenging to determine accurately using X-ray scattering due to low scattering power of Li compared to the heavier elements in the structure. Neutron diffraction data would possibly provide a more accurate result for the Li ion occupancy, as obtained previously for the isostructural compound $\text{LiCe}(\text{BH}_4)_3\text{Cl}$.¹³ The orientation of the BH_4^- groups is adopted from structural refinement of $\text{LiCe}(\text{BH}_4)_3\text{Cl}$ using PND, data and the Li^+ ions coordinate tetrahedrally to four BH_4^- groups. The BH_4^- group is coordinated via the face by the heavy atoms ($\text{BH}_3 \cdots \text{M}$ coordination scheme for $\text{M} = \text{La}, \text{Gd}$) and via a tetrahedral edge by Li^+ , i.e., $\text{BH}_2 \cdots \text{Li}$ coordination scheme.

Ionic and Electronic Conductivities. Electrical conductivities of the samples $\text{LaCl}_3\text{-LiBH}_4$ (1:3, s4) and $\text{GdCl}_3\text{-LiBH}_4$ (1:3, s5) were measured by electrochemical impedance spectroscopy, at $T = 20^\circ\text{C}$. Figure 3 reveals Warburg

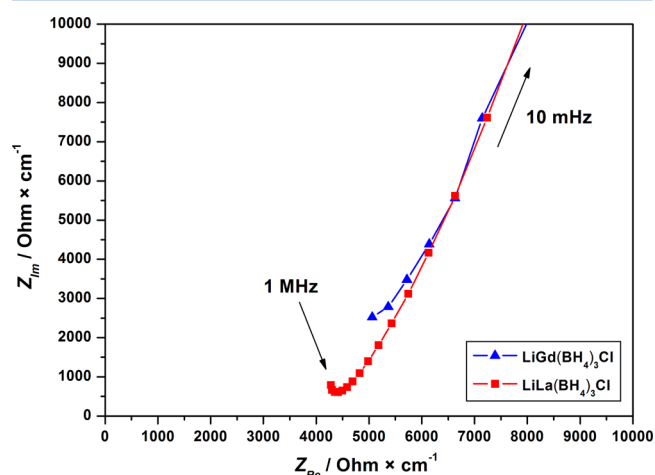


Figure 3. Complex impedance spectra for $\text{LaCl}_3\text{-LiBH}_4$ (1:3, s4) and $\text{GdCl}_3\text{-LiBH}_4$ (1:3, s5) recorded at $T = 20^\circ\text{C}$.

impedances related to the semi-infinite diffusion at the electrodes for both samples. In the case of La, the beginning of a semicircle assigned to the lithium ion mobility can be seen at high frequencies; as a matter of fact, frequencies higher than 1 MHz would be needed to fully plot this semicircle. The shapes of the observed impedance spectra are typical for good conductors, and conductivities can be calculated from the intercepts with the real axis (Z_{re}). Ionic conductivities of 2.3×10^{-4} and $3.5 \times 10^{-4} \text{ S}\cdot\text{cm}^{-1}$ are found at 20°C for $\text{LiLa}(\text{BH}_4)_3\text{Cl}$ and $\text{LiGd}(\text{BH}_4)_3\text{Cl}$, respectively. These values are slightly higher than the conductivity of $1.0 \times 10^{-4} \text{ S}\cdot\text{cm}^{-1}$ previously reported for $\text{LiCe}(\text{BH}_4)_3\text{Cl}$ and are much higher than that measured for $o\text{-LiBH}_4$, $8.6 \times 10^{-8} \text{ S}\cdot\text{cm}^{-1}$ at $T = 20^\circ\text{C}$, using the same experimental conditions.²⁵ As a comparison, the impedance spectra recorded for LiBH_4 is shown in the Supporting Information (Figure S3). From the diameter of the semicircle observed at high frequency, which is related to the lithium ion mobility, a conductivity of $8.6 \times 10^{-8} \text{ S}\cdot\text{cm}^{-1}$ is found in good agreement with the values reported for orthorhombic $o\text{-LiBH}_4$. The conductivities of the $\text{LiM}(\text{BH}_4)_3\text{Cl}$, $\text{M} = \text{La}, \text{Ce},$ or Gd , samples are therefore more than 3 orders of magnitude higher than that of $o\text{-LiBH}_4$ at RT and are similar to that found for the hexagonal $h\text{-LiBH}_4\text{-LiI}$ solid solution.⁴⁰

Temperature-dependent conductivity measurements were also performed for $\text{LiM}(\text{BH}_4)_3\text{Cl}$ ($\text{M} = \text{La}$ or Gd) samples. The complex impedance spectra recorded for $\text{LaCl}_3\text{-LiBH}_4$ (1:3, s4) and $\text{GdCl}_3\text{-LiBH}_4$ (1:3, s5) can be found in Figure S4 and Figure S5 (Supporting Information), respectively. For both samples, the resistance rapidly decreases when increasing the temperature. Figure 4 presents the evolution of the

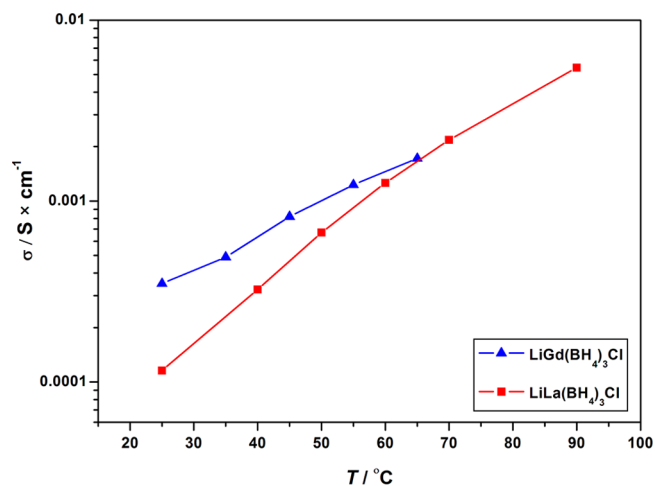


Figure 4. Electric conductivities of $\text{LaCl}_3\text{-LiBH}_4$ (1:3, s4) and $\text{GdCl}_3\text{-LiBH}_4$ (1:3, s5) as a function of the temperature.

electrical conductivities for $\text{LiLa}(\text{BH}_4)_3\text{Cl}$ and $\text{LiGd}(\text{BH}_4)_3\text{Cl}$. The lanthanum containing compound has ionic conductivity of $5.5 \times 10^{-3} \text{ S}\cdot\text{cm}^{-1}$ at 90°C , which may exceed $1 \times 10^{-2} \text{ S}\cdot\text{cm}^{-1}$ at $T \sim 100^\circ\text{C}$. The conductivities follow a linear Arrhenius behavior when $\ln(\sigma T)$ is plotted as a function of $1/T$ as depicted in Figure 5. From the slope of the linear fittings,

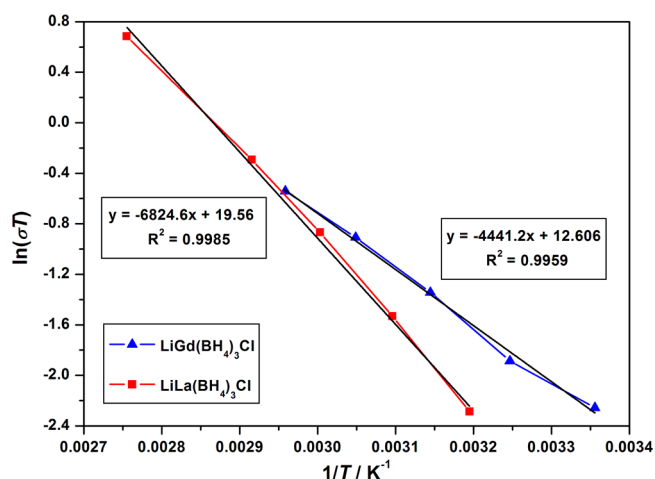


Figure 5. Arrhenius plots of the electric conductivities of $\text{LaCl}_3\text{-LiBH}_4$ (1:3, s4) and $\text{GdCl}_3\text{-LiBH}_4$ (1:3, s5).

activation energies, $E_a = 57 \text{ kJ}\cdot\text{mol}^{-1}$ (0.59 eV) and $37 \text{ kJ}\cdot\text{mol}^{-1}$ (0.38 eV), are found for $\text{LiLa}(\text{BH}_4)_3\text{Cl}$ and $\text{LiGd}(\text{BH}_4)_3\text{Cl}$, respectively. The latter E_a value is lower than those reported for LiBH_4 ($E_a = 66 \text{ kJ}\cdot\text{mol}^{-1}$ (0.69 eV) and $51 \text{ kJ}\cdot\text{mol}^{-1}$ (0.53 eV) for the orthorhombic LT and the hexagonal HT polymorph, respectively), and this highlights the high mobility of the Li^+ cations within the newly reported crystal structure of $\text{LiGd}(\text{BH}_4)_3\text{Cl}$.

To demonstrate that the conductivity is purely ionic, direct current conductivity experiments were performed at $T = 20\text{ }^{\circ}\text{C}$ for both $\text{LaCl}_3\text{-LiBH}_4$ (1:3, **s4**) and $\text{GdCl}_3\text{-LiBH}_4$ (1:3, **s5**), which provide the electronic conductivities using Ohm's law. Figure S6 in the Supporting Information shows linear evolutions of the current I when increasing the applied voltage $U = 2.0, 2.5,$ and 3.0 V . From the slopes of the ohmic plots, resistances of $23\,300$ and $3040\text{ k}\Omega$ are obtained, which corresponds to electronic conductivities of 1.4×10^{-8} and $9 \times 10^{-8}\text{ S}\cdot\text{cm}^{-1}$ for pellets ($\varnothing = 10\text{ mm}$, thickness = 2.65 and 2.17 mm) for $\text{LiLa}(\text{BH}_4)_3\text{Cl}$ and $\text{LiGd}(\text{BH}_4)_3\text{Cl}$, respectively. The electronic conductivities are therefore about 4 orders of magnitude lower than the ionic conductivities found from the impedance spectroscopy experiments. This confirms that the electric conductivity measured for $\text{LiM}(\text{BH}_4)_3\text{Cl}$ ($M = \text{La}$ or Gd) samples solely originates from the high mobility of Li^+ .

These conductivity measurements suggest that the $\text{LiM}(\text{BH}_4)_3\text{Cl}$ compounds could be considered as promising materials for solid electrolytes in lithium-ion batteries. Electrochemical cycling at low temperatures ($T < 100\text{ }^{\circ}\text{C}$) of all solid-state lithium-ion batteries using the $\text{MCl}_3\text{-LiBH}_4$ (1:3) ball-milled samples as electrolytes is in progress to demonstrate such a feasibility. Furthermore, the conductivity measurements reported in this study were performed on pellets, which were composed of $\text{LiM}(\text{BH}_4)_3\text{Cl}$ and LiCl 1:2 (see eqs 1–3). Higher conductivities are expected for a sample of pure $\text{LiM}(\text{BH}_4)_3\text{Cl}$, since LiCl is a nonconducting material.

Thermal Analysis and Sieverts Measurements. The sample $\text{LaCl}_3\text{-LiBH}_4$ (1:3, **s4**) was studied by simultaneous TGA/DTA/MS and DSC (see Figures 6 and 8). TGA shows

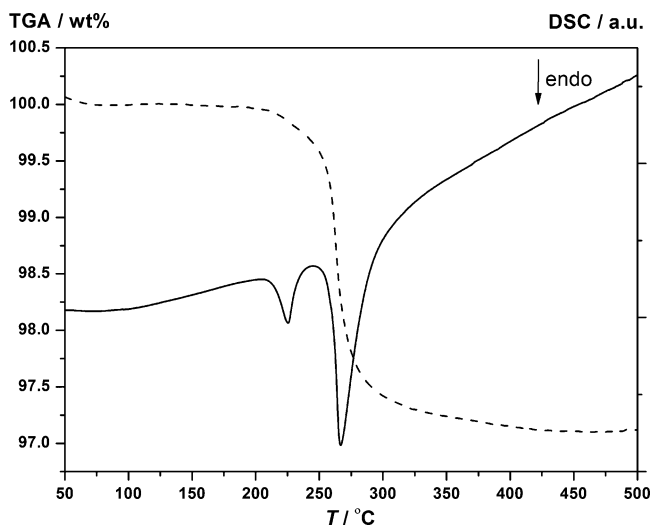


Figure 6. Thermogravimetric analysis, TGA (dash), and differential thermal analysis, DSC (full), measured for $\text{LaCl}_3\text{-LiBH}_4$ (1:3, **s4**) in the temperature range RT to $500\text{ }^{\circ}\text{C}$ ($\Delta T/\Delta t = 10\text{ }^{\circ}\text{C}/\text{min}$ in Ar flow).

that a mass loss of $2.87\text{ wt}\%$ is observed in the temperature range $200\text{--}400\text{ }^{\circ}\text{C}$, which is $1\text{ wt}\%$ smaller than the theoretical hydrogen content for the sample, $3.89\text{ wt}\%$ H_2 (including LiCl). The onset of the mass loss is associated with a smaller endothermic peak at $226\text{ }^{\circ}\text{C}$. A larger endothermic DSC event is observed with peak value at $266\text{ }^{\circ}\text{C}$ associated with the main mass loss from the decomposition of $\text{LiLa}(\text{BH}_4)_3\text{Cl}$. Mass spectroscopy measurement reveals that hydrogen is released in the temperature range $226\text{--}300\text{ }^{\circ}\text{C}$ with a smaller amount with

maximum release rate at $226\text{ }^{\circ}\text{C}$ and a larger amount at $266\text{ }^{\circ}\text{C}$. There is no indication of contaminating borane species, i.e., B_2H_6 (no peak is detected for $m/z = 28$).

Simultaneous TGA/DTA/MS and separately recorded DSC for sample $\text{GdCl}_3\text{-LiBH}_4$ (1:3, **s5**) (see Figures 7 and 8) reveal

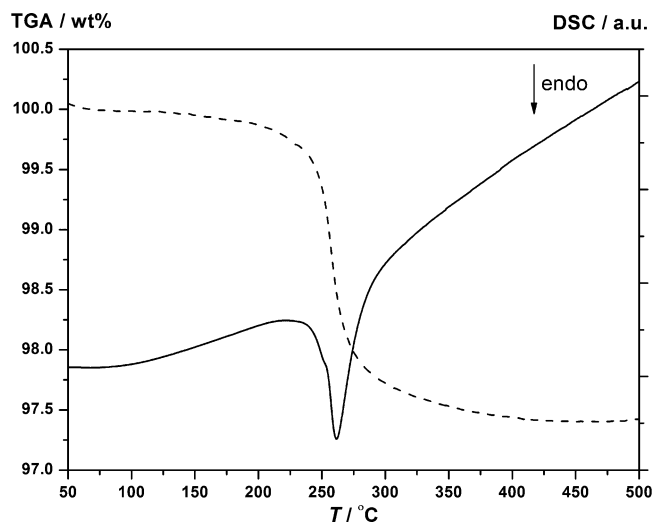


Figure 7. Thermogravimetric analysis, TGA (dash), and differential thermal analysis, DSC (full), measured for $\text{GdCl}_3\text{-LiBH}_4$ (1:3, **s5**) in the temperature range RT to $500\text{ }^{\circ}\text{C}$ ($\Delta T/\Delta t = 10\text{ }^{\circ}\text{C}/\text{min}$ in Ar flow).

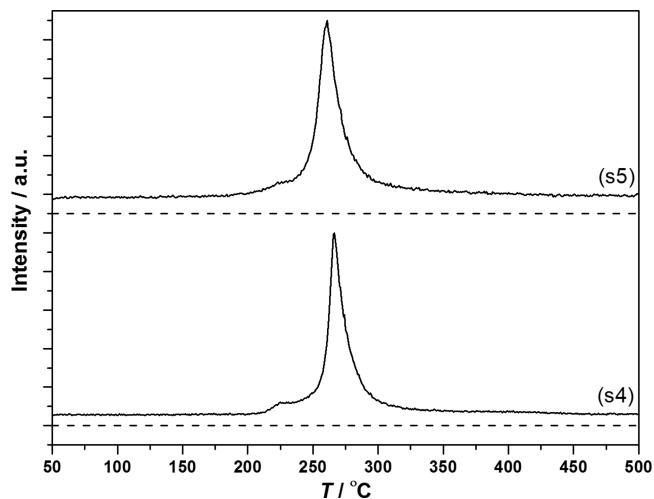


Figure 8. Mass spectroscopy signal showing hydrogen release ($m/z = 2$, full) and diborane, B_2H_6 ($m/z = 28$, dash), for $\text{LaCl}_3\text{-LiBH}_4$ (1:3, **s4**) and $\text{GdCl}_3\text{-LiBH}_4$ (1:3, **s5**) using a heating rate of $\Delta T/\Delta t = 10\text{ }^{\circ}\text{C}/\text{min}$.

that hydrogen is released in a single step at $261\text{ }^{\circ}\text{C}$. TGA reveals a mass loss in the temperature range $200\text{--}450\text{ }^{\circ}\text{C}$ of $2.58\text{ wt}\%$, which is again smaller than the theoretical hydrogen content of $3.67\text{ wt}\%$ for the sample (including LiCl). DSC reveals one major endothermic event at $261\text{ }^{\circ}\text{C}$ with a minor shoulder at $250\text{ }^{\circ}\text{C}$. Previous investigations of the $\text{GdCl}_3\text{-LiBH}_4$ system also shows this shoulder, which indicates multiple reactions during decomposition.²⁹

Mass spectroscopy data confirm that only hydrogen is released with a minor peak at $225\text{ }^{\circ}\text{C}$ and a major peak at $275\text{ }^{\circ}\text{C}$, apparently without contaminating borane species. The discrepancy between the two samples **s4** and **s5** may originate

from differences in the preparation procedure, where the samples have been heated to 200 and 220 °C in the case of $\text{LiLa}(\text{BH}_4)_3\text{Cl}$ and $\text{LiGd}(\text{BH}_4)_3\text{Cl}$, respectively. A previous study of the $\text{GdCl}_3\text{--LiBH}_4$ system, where the sample was not preheated prior to the DSC experiment, revealed an endothermic peak at 211 °C.²⁹ Additionally, unreacted LiBH_4 left from ball-milling might be catalyzed by the remaining metal chlorides in the sample and release hydrogen in the same temperature range as the novel compounds $\text{LiLa}(\text{BH}_4)_3\text{Cl}$ and $\text{LiGd}(\text{BH}_4)_3\text{Cl}$.²⁸ However, thermal treatment of the samples lead to further formation of $\text{LiM}(\text{BH}_4)_3\text{Cl}$, $M = \text{La}$ or Gd ; i.e., the remaining LiBH_4 and LaCl_3 or GdCl_3 is consumed prior to decomposition of $\text{LiM}(\text{BH}_4)_3\text{Cl}$ (which is further discussed later in this paper).

Hydrogen storage properties were investigated using Sieverts (PCT) measurements for samples **s1**, **s2**, and **s3** (Figure 9).

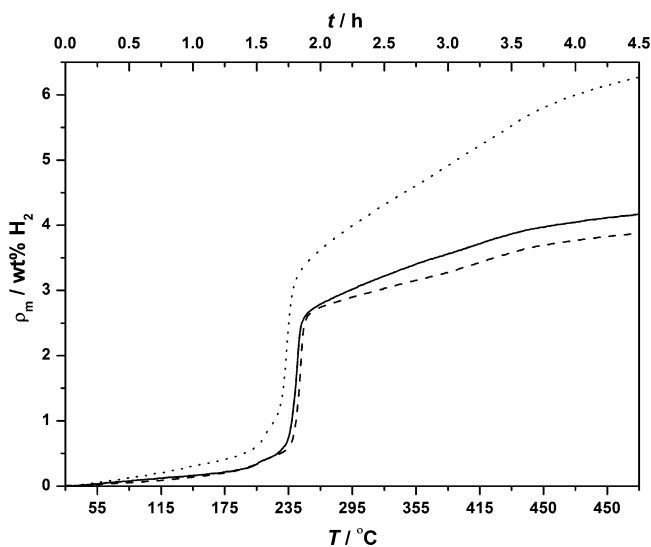


Figure 9. Sieverts measurement of $\text{LaCl}_3\text{--LiBH}_4$ (1:3, **s1**, solid line), $\text{GdCl}_3\text{--LiBH}_4$ (1:3, **s2**, dash), and solvent-extracted $\text{Gd}(\text{BH}_4)_3$ (**s3**, dot) showing the first desorption conducted in the temperature range RT to 450 °C ($\Delta T/\Delta t = 2$ °C/min and $p(\text{H}_2) = 1$ bar).

Hydrogen absorption was not possible at the selected physical p, T conditions for our studies as shown later by FTIR and PXD. During the first desorption in the Sievert's measurement, all three samples release 0.3–0.55 wt % H_2 from RT to 200 °C (possibly from an unidentified gas). However, no mass loss or hydrogen evolution is observed in any of the TGA/MS experiments.

The gravimetric and volumetric hydrogen densities in $\text{LiLa}(\text{BH}_4)_3\text{Cl}$ are $\rho_m = 5.36$ wt % H_2 and $\rho_v = 96.4$ kg H_2/m^3 , respectively. Sample **s1** releases 0.17 wt % H_2 from 200 to 225 °C, and a major H_2 release of 2.2 wt % H_2 is observed from 225 to 270 °C. Throughout the heating to 450 °C and the following isotherm at 450 °C, 1.5 wt % H_2 is additionally released, raising the total mass loss to 3.87 wt % H_2 , corresponding well to the theoretical hydrogen content of the sample of 3.9 wt % H_2 .

The gravimetric and volumetric hydrogen densities in $\text{LiGd}(\text{BH}_4)_3\text{Cl}$ are $\rho_m = 4.95$ wt % H_2 and $\rho_v = 102.6$ kg H_2/m^3 , respectively. Sample **s2** also releases 0.17 wt % H_2 from 200 to 225 °C, and a major H_2 release of 2.15 wt % H_2 is observed from 225 to 250 °C. A total of 1.25 wt % H_2 is released from **s2** during the final heating to 450 °C and the

following isotherm at 450 °C, giving a total mass loss of 3.6 wt %, which also compares well to the theoretical hydrogen content of 3.7 wt % for the sample. The observed desorption temperatures confirm that the hydrogen storage properties of $\text{LiLa}(\text{BH}_4)_3\text{Cl}$ and $\text{LiGd}(\text{BH}_4)_3\text{Cl}$ are indeed very similar, possibly due to similar electronegativities for lanthanum and gadolinium and that the two compounds are isostructural. The mass loss observed in the Sieverts measurement for **s2** is larger than the mass loss observed for **s2** in the TGA/DTA experiment. The difference may originate from the use of a slower heating rate. Additionally, the isotherm at 450 °C applied in the Sieverts measurement facilitates a more complete desorption, where the metal hydride produced from the decomposition of the parent metal borohydride may also decompose.

The solvent-extracted sample of $\text{Gd}(\text{BH}_4)_3$ (**s3**) releases 0.6 wt % H_2 from 200 to 225 °C compared to 0.2 wt % H_2 for the ball-milled sample. From 225 to 250 °C, the sample releases 2.35 wt % H_2 and additionally 2.8 wt % H_2 at higher temperatures, providing a total mass loss of 5.75 wt % H_2 , which is comparable to the total hydrogen content $\rho_m(\text{Gd}(\text{BH}_4)_3) = 5.99$ wt % H_2 . Indeed, the removal of LiCl facilitates the full hydrogen desorption capability of $\text{Gd}(\text{BH}_4)_3$. An interesting observation is that the onset temperatures are similar, 200 or 225 °C, respectively, for the different steps in the decomposition. No measurable difference in the onset temperatures is observed between the two samples containing gadolinium, even though most of the LiCl has been removed from the solvent-extracted sample. Indeed, the reduced formation of the novel compound $\text{LiGd}(\text{BH}_4)_3\text{Cl}$ does not have an effect on the decomposition temperature or the steps in the decomposition. In both samples, the decomposition takes place in a two-step mechanism, a small mass loss followed by a rather abrupt mass loss in a very narrow temperature range of 25 °C.

Infrared Spectroscopy. The samples **s1**, **s3**, and **s5** were further investigated by Fourier transform infrared spectroscopy (FTIR), as shown in Figure S8 (Supporting Information). The FTIR spectrum for **s1** reveals the signatures of $[\text{BH}_4^-]$ bending modes at 1092 cm^{-1} and stretching at 2305 cm^{-1} , which are located in the typical B–H vibrational range for borohydrides and are expected to originate from the $\text{LiLa}(\text{BH}_4)_3\text{Cl}$ compound. The FTIR spectrum of sample **s5** shows that when an as-milled sample of $\text{GdCl}_3\text{--LiBH}_4$ (1:3) is heated to produce $\text{LiGd}(\text{BH}_4)_3\text{Cl}$ the stretching and bending modes of the borohydride group are less intense. However, signatures of $[\text{BH}_4^-]$ bending modes at 1184 cm^{-1} and stretching at 2259 cm^{-1} reveal that the borohydride chloride is still present. Additionally, the FTIR spectrum of the solvent-extracted sample of $\text{Gd}(\text{BH}_4)_3$ shows that some ether solvent remains in the sample after extraction, as revealed by the C–H stretching modes at 2922 cm^{-1} and bending at 1185 cm^{-1} . However, as for the two other samples, $[\text{BH}_4^-]$ bending modes at 1123 cm^{-1} and stretching at 2263 cm^{-1} reveal the presence of the borohydride group in $\text{Gd}(\text{BH}_4)_3$. The presence of diethyl ether in a form of crystalline complexes is not detected in any of the diffraction experiments. The samples used in the Sieverts measurement were also studied using FTIR spectroscopy (see Figure S9, Supporting Information). A minor and broad absorption is observed in the spectrum for **s3** at 1373 cm^{-1} , which was not assigned. No bending or stretching modes are observed for the two other samples, confirming that the

physical conditions applied here for hydrogen absorption are not sufficient to allow formation of borohydrides.

Decomposition Mechanisms Observed by in situ SR-PXD. The thermal decompositions of samples $\text{LaCl}_3\text{-LiBH}_4$ (1:3, **s1**), $\text{GdCl}_3\text{-LiBH}_4$ (1:3, **s2**), and $\text{Gd}(\text{BH}_4)_3$ (**s3**) were studied by in situ SR-PXD (see Figures 10, 11, and 12). The

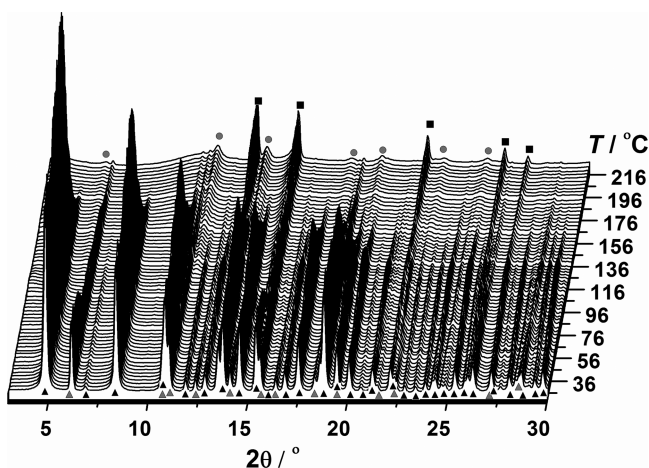


Figure 10. In situ SR-PXD data for $\text{LaCl}_3\text{-LiBH}_4$ (1:3, **s1**) measured from RT to 220 °C ($\Delta T/\Delta t = 1$ °C/min, $p(\text{Ar}) = 1$ bar, $\lambda = 0.69736$ Å). Symbols: black triangle, $\text{LiLa}(\text{BH}_4)_3\text{Cl}$; gray triangle, LaCl_3 ; black box, LiCl ; and gray circle, Unknown 1.

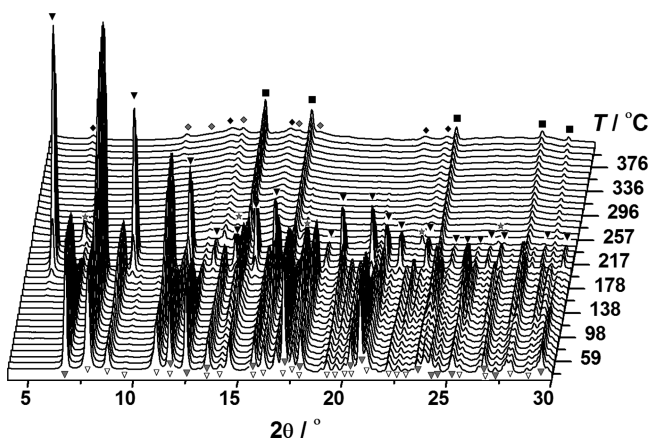


Figure 11. In situ SR-PXD data for $\text{GdCl}_3\text{-LiBH}_4$ (1:3, **s2**) measured from RT to 400 °C ($\Delta T/\Delta t = 5$ °C/min, $p(\text{Ar}) = 1$ bar, $\lambda = 0.75277$ Å). Symbols: open down triangle, $\text{Gd}(\text{BH}_4)_3$; gray down triangle, GdCl_3 ; black down triangle, $\text{LiGd}(\text{BH}_4)_3\text{Cl}$; black box, LiCl ; gray diamond, GdB_4 ; gray star, Unknown 2; and black diamond, Unknown 3.

first SR-PXD pattern in the series for **s1** (Figure 10) measured at RT shows diffraction peaks from $\text{LiLa}(\text{BH}_4)_3\text{Cl}$, LaCl_3 , and LiCl . LaCl_3 remains in the sample during the complete heating run, but peaks corresponding to lanthanum chloride decrease in intensity at $T > 50$ °C. Above 50 °C, the diffracted peak intensity from $\text{LiLa}(\text{BH}_4)_3\text{Cl}$ increases due to the continuation of reaction eq 1. The Bragg diffraction peaks from $\text{LiLa}(\text{BH}_4)_3\text{Cl}$ disappear at 185 °C due to melting corresponding to results from TGA/MS and DSC measurements where decomposition was observed at $T \sim 266$ °C. Melting of $\text{LiLa}(\text{BH}_4)_3\text{Cl}$ is correlated with a minor increase in the diffracted intensity from LiCl . Diffraction peaks from an unknown compound appear at 165 °C. The unknown

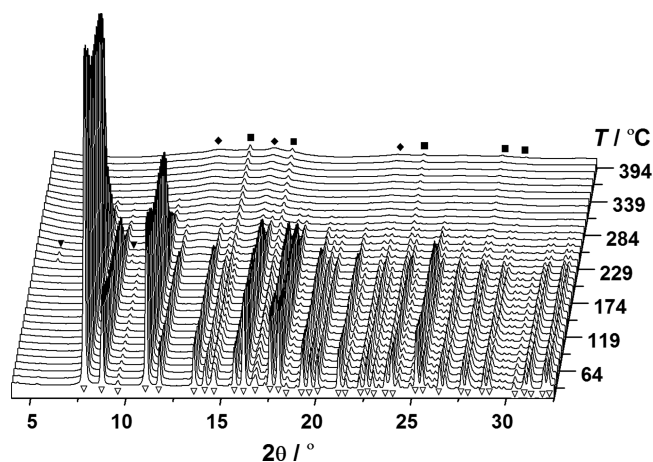
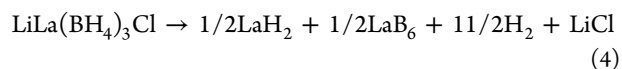


Figure 12. In situ SR-PXD data for solvent-extracted $\text{Gd}(\text{BH}_4)_3$ (**s3**) measured from RT to 400 °C ($\Delta T/\Delta t = 5$ °C/min, $p(\text{Ar}) = 1$ bar, $\lambda = 0.753377$ Å). Symbols: open down triangle, $\text{Gd}(\text{BH}_4)_3$; black down triangle, $\text{LiGd}(\text{BH}_4)_3\text{Cl}$; black box, LiCl ; and black diamond, Unknown 3.

compound may be a ternary salt, which may explain the decreasing diffracted intensity from LiCl in this region. A ternary salt, NaYCl_4 , is also observed during the decomposition of $\text{NaY}(\text{BH}_4)_2\text{Cl}_2$.¹¹ Sample **s1** used in the Sieverts measurement was studied using PXD after the absorption experiment (see Figure S10, Supporting Information). Lanthanum hydride and lanthanum boride, LaH_2 and LaB_6 , were observed, which lead to a reaction scheme (eq 4) as a possible overall decomposition reaction for $\text{LiLa}(\text{BH}_4)_3\text{Cl}$. The unknown/unidentified compound **1** may form in a side reaction.



Initially, $\text{Gd}(\text{BH}_4)_3$, GdCl_3 , and LiCl are present at RT in sample **s2** (see Figure 11). When the temperature reaches 80 °C, the diffracted intensity from $\text{Gd}(\text{BH}_4)_3$ and LiCl starts to increase in intensity, and simultaneously the GdCl_3 peak intensity decreases according to eq 2. At 200 °C, $\text{Gd}(\text{BH}_4)_3$ reacts with LiCl , forming $\text{LiGd}(\text{BH}_4)_3\text{Cl}$ according to eq 3. This is also associated with a decrease in intensity of the Bragg peaks belonging to LiCl . At 240 °C, diffraction peaks from $\text{LiGd}(\text{BH}_4)_3\text{Cl}$ vanish due to decomposition, simultaneous with formation of an unknown compound **2** (see Figure 11). Bragg peaks from **2** can be indexed by a monoclinic unit cell, $a = 7.76(1)$, $b = 12.71(5)$, $c = 3.62(1)$ Å, and $\beta = 94.7(2)^\circ$. However, structure solution has not yet been possible. Bragg peaks from **2** disappear at 290 °C. At the end of the heating, peaks from GdB_4 and an unknown compound **3** appear (see Figure 11). Compound **3** has peak positions similar to **1** observed in the La system, and the two compounds may be structurally related.

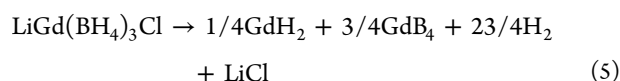
A PXD diagram at RT of solvent-extracted $\text{Gd}(\text{BH}_4)_3$ is shown in Figure S7 (Supporting Information). However, in situ SR-PXD data from **s3** reveal that the diffracted intensity for $\text{Gd}(\text{BH}_4)_3$ decreases at $T > 180$ °C, but $\text{Gd}(\text{BH}_4)_3$ remains in the sample until 270 °C (see Figure 12). Small peaks indicating the formation of $\text{LiGd}(\text{BH}_4)_3\text{Cl}$ are observed at 220 °C. Compound **3** appears toward the end of the heating in **s3**. After the Sieverts measurement, **s2** and **s3** were studied by PXD to acquire information on the decomposition products (see Figure S10, Supporting Information). In sample **s2**, only LiCl and **3**

Table 2. Hydrogen Densities, Decomposition Temperatures and Conductivities for the Three Compounds $\text{LiM}(\text{BH}_4)_3\text{Cl}$ ($\text{M} = \text{La, Ce, or Gd}$)

compound	unit cell	ρ_m^a	ρ_v^a	T_{dec}^b	Li-ion	electronic
	$a/\text{\AA}$	wt % H_2	$\text{kg H}_2 \text{ m}^{-3}$	$^\circ\text{C}$	$\times 10^{-4} \text{ S}\cdot\text{cm}^{-1}$	$\times 10^{-8} \text{ S}\cdot\text{cm}^{-1}$
$\text{LiLa}(\text{BH}_4)_3\text{Cl}$	11.7955(1)	5.36	96.4	266 ± 2	2.3 ± 0.6	1.4 ± 0.1
$\text{LiCe}(\text{BH}_4)_3\text{Cl}$	11.7204(2)	5.33	99.8	258 ± 2	1.0 ± 0.3	-
$\text{LiGd}(\text{BH}_4)_3\text{Cl}$	11.5627(1)	4.95	102.6	261 ± 2	3.6 ± 0.6	9 ± 0.9

^aCalculated values. ^bValues from thermogravimetric experiments.

are observed. Crystalline GdB_4 is also observed in sample **s3** together with LiCl . Gadolinium hydride GdH_2 is not observed to crystallize in any of the in situ SR-PXD studies and is neither observed in **s2** nor **s3** after the rehydrogenation in the Sieverts measurement, but GdH_2 is reported to form in previous studies. The reaction scheme in eq 5 describes the overall idealized decomposition reaction for $\text{LiGd}(\text{BH}_4)_3\text{Cl}$. The unknown or unidentified compounds **2** and **3** may form in side reactions.



Comparison with Related Compounds. For $\text{LiCe}(\text{BH}_4)_3\text{Cl}$, the position of the Li^+ ions was discovered by the combined use of powder X-ray and neutron diffraction and DFT optimization. After considering several models for the structure, the Li^+ ions were positioned on the $12d$ Wyckoff site with an idealized occupancy of $2/3$.¹³ DFT optimization indicates that the $\text{LiCe}(\text{BH}_4)_3\text{Cl}$ structure is stabilized by higher entropy rather than lower enthalpy. The Li disorder may be the origin of the high Li-ion conductivity observed for the whole $\text{LiM}(\text{BH}_4)_3\text{Cl}$ series of compounds, $\text{M} = \text{La, Ce, Gd}$. Lanthanum and cerium have similar ionic radii, for the same coordination number (6) and oxidation state of (3+), 1.04 and 1.02 Å, respectively, which may explain the formation of the isostructural compounds (see Table 2). However, the formation of $\text{LiGd}(\text{BH}_4)_3\text{Cl}$ is more intriguing as gadolinium has a smaller ionic radius (0.94 Å). $\text{Gd}(\text{BH}_4)_3$ forms during BM at RT from the same reaction mechanism as observed for the formation of $\alpha\text{-Y}(\text{BH}_4)_3$. When heated, $\alpha\text{-Y}(\text{BH}_4)_3$ transforms into the high-temperature polymorph $\beta\text{-Y}(\text{BH}_4)_3$ at 190 °C.^{41,42} In contrast, $\text{Gd}(\text{BH}_4)_3$ does not form a high-temperature polymorph when heated but reacts with LiCl at 193 °C and forms $\text{LiGd}(\text{BH}_4)_3\text{Cl}$, thus resembling both the systems with larger (Ce, La) and smaller (Y) ions. The size factor is crucial for the phase stability in $\text{LiBH}_4\text{-MCl}_3$ systems.

CONCLUSION

The novel compounds, $\text{LiLa}(\text{BH}_4)_3\text{Cl}$ and $\text{LiGd}(\text{BH}_4)_3\text{Cl}$, crystallize in the cubic crystal system with the space group $I\bar{4}3m$, and the structure contains isolated tetranuclear anionic clusters $[\text{M}_4\text{Cl}_4(\text{BH}_4)_{12}]^{4-}$ with a distorted cubane M_4Cl_4 ($\text{M} = \text{La, Gd}$) core charge-balanced by Li^+ cations. The Li^+ ions are disordered and occupy $2/3$ of the $12d$ Wyckoff sites in accord with high lithium ion conductivities of 2.3×10^{-4} and $3.5 \times 10^{-4} \text{ S}\cdot\text{cm}^{-1}$ at $T = 20$ °C and low activation energies of 57 and only 37 $\text{kJ}\cdot\text{mol}^{-1}$ for $\text{LiLa}(\text{BH}_4)_3\text{Cl}$ and $\text{LiGd}(\text{BH}_4)_3\text{Cl}$, respectively. This low activation energy accounts for an ionic conductivity exceeding $10^{-3} \text{ S}\cdot\text{cm}^{-1}$ for $\text{LiGd}(\text{BH}_4)_3\text{Cl}$ at a temperature as low as 50 °C. The conductivity is purely ionic as low electronic conductivities of 1.4×10^{-8} and $9 \times 10^{-8} \text{ S}\cdot\text{cm}^{-1}$ at $T = 20$ °C were measured for $\text{LiLa}(\text{BH}_4)_3\text{Cl}$ and $\text{LiGd}(\text{BH}_4)_3\text{Cl}$, respectively. The two new compounds LiLa

$(\text{BH}_4)_3\text{Cl}$ and $\text{LiGd}(\text{BH}_4)_3\text{Cl}$ store 5.36 and 4.99 wt % H_2 , respectively, which is released in the temperature range 200–400 °C. The solvent extracted sample of $\text{Gd}(\text{BH}_4)_3$ releases 5.75 wt % H_2 and shows that the purification process indeed removes a high fraction of the LiCl formed during ball-milling. The reversible hydrogen storage properties for rare earth metal borohydrides may benefit from the solvent extraction process as the total hydrogen content becomes available and formation of ternary chlorides may be avoided. This may also be important in reactive hydride composite based on rare earth metal borohydrides, which remains an unexplored area of solid state hydrogen storage.

ASSOCIATED CONTENT

Supporting Information

Additional tables and figures. This material is available free of charge via the Internet at <http://pubs.acs.org>.

AUTHOR INFORMATION

Corresponding Author

*E-mail: trj@chem.au.dk. Tel.: +45 8942 3894. Fax: +45 8619 6199.

Notes

The authors declare no competing financial interest.

ACKNOWLEDGMENTS

We thank the Danish Natural Science Research Councils for funding the research program; DanScatt and the Danish Strategic Research Council's Center for Energy Materials (CEM); and the project HyFillFast. We also thank Center for Materials Crystallography (CMC) funded by The Danish National Research Foundation for support. R. Janot and S. Boulineau gratefully acknowledge M. Courty (LRCS, Amiens) for the thermal analysis done on the different samples.

REFERENCES

- (1) MacKay, D. J. C. *Sustainable Energy - without the hot air*; UIT: Cambridge, 2009.
- (2) Fichtner, M. J. *Alloys Compd.* **2011**, *S09*, S29–S34.
- (3) Li, H. W.; Yan, Y.; Orimo, S.; Züttel, A.; Jensen, C. M. *Energies* **2011**, *4*, 185–214.
- (4) Orimo, S.; Nakamori, Y.; Eliseo, J. R.; Züttel, A.; Jensen, C. M. *Chem. Rev.* **2007**, *107*, 4111–4132.
- (5) Grochala, W.; Edwards, P. P. *Chem. Rev.* **2004**, *104*, 1283–1316.
- (6) Ravnsbæk, D. B.; Filinchuk, Y.; Cerný, R.; Jensen, T. R. Z. *Kristallogr.* **2010**, *225*, 557–569.
- (7) Rude, L. H.; Nielsen, T. K.; Ravnsbæk, D. B.; Bösenberg, U.; Ley, M. B.; Richter, B.; Arnbjerg, L. M.; Dornheim, M.; Filinchuk, Y.; Besenbacher, F.; Jensen, T. R. *Phys. Status Solidi A* **2011**, *208*, 1754–1773.
- (8) Nakamori, Y.; Li, H.-W.; Kikuchi, K.; Aoki, M.; Miwa, K.; Towata, S.; Orimo, S. J. *Alloys Compd.* **2007**, *446–447*, 296–300.
- (9) Züttel, A.; Borgschulte, A.; Orimo, S. I. *Scr. Mater.* **2007**, *56*, 823–828.

- (10) Ravnsbæk, D. B.; Sørensen, L. H.; Filinchuk, Y.; Besenbacher, F.; Jensen, T. R. *Angew. Chem., Int. Ed.* **2012**, *51*, 3582–3586.
- (11) Ravnsbæk, D. B.; Ley, M. B.; Lee, Y. S.; Hagemann, H.; D'Anna, V.; Cho, Y. W.; Filinchuk, Y.; Jensen, T. R. *Int. J. Hydrogen Energy* **2012**, *37*, 8428–8438.
- (12) Frommen, C.; Sørby, M. H.; Ravindran, P.; Vajeeston, P.; Fjellvåg, H.; Hauback, B. C. *J. Phys. Chem. C* **2011**, 23591–23602.
- (13) Ley, M. B.; Ravnsbæk, D. B.; Filinchuk, Y.; Lee, Y.-S.; Janot, R.; Cho, Y. W.; Skibsted, J.; Jensen, T. R. *Chem. Mater.* **2012**, *24*, 1654–1663.
- (14) Hagemann, H.; Longhini, M.; Kaminski, J. W.; Wesolowski, T. A.; Černý, R.; Penin, N.; Sørby, M. H.; Hauback, B. C.; Severa, G.; Jensen, C. M. *J. Phys. Chem. A* **2008**, *112*, 7551–7555.
- (15) Kim, C.; Hwang, S.-J.; Bowman, R. C.; Reiter, J. W.; Zan, J. A.; Kulleck, J. G.; Kabbour, H.; Majzoub, E. H.; Ozolins, V. *J. Phys. Chem. C* **2009**, *113*, 9956–9968.
- (16) Černý, R.; Severa, G.; Ravnsbæk, D. B.; Filinchuk, Y.; d'Anna, V.; Hagemann, H.; Haase, D.; Jensen, C. M.; Jensen, T. R. *J. Phys. Chem. C* **2010**, *114*, 1357–1364.
- (17) Černý, R.; Ravnsbæk, D. B.; Severa, G.; Filinchuk, Y.; D'Anna, V.; Hagemann, H.; Haase, D.; Skibsted, J.; Jensen, C. M.; Jensen, T. R. *J. Phys. Chem. C* **2010**, *114*, 19540–19549.
- (18) Jaroń, T.; Grochala, W. *Dalton Trans.* **2011**, *40*, 12808–12817.
- (19) Züttel, A.; Rentsch, S.; Fischer, P.; Wenger, P.; Sudan, P.; Mauron, P.; Emmenegger, C. *J. Alloys Compd.* **2003**, 356–357, 515–520.
- (20) Mosegaard, L.; Møller, B.; Jørgensen, J.-E.; Filinchuk, Y.; Cerenius, Y.; Hanson, J. C.; Dimasi, E.; Besenbacher, F.; Jensen, T. R. *J. Phys. Chem. C* **2008**, *112*, 1299–1303.
- (21) Arnbjerg, L. M.; Ravnsbæk, D. B.; Filinchuk, Y.; Vang, R. T.; Cerenius, Y.; Besenbacher, F.; Jørgensen, J.-E.; Jakobsen, H. J.; Jensen, T. R. *Chem. Mater.* **2009**, *21*, 5772–5782.
- (22) Rude, L. H.; Groppo, E.; Arnbjerg, L. M.; Ravnsbæk, D. B.; Malmkjær, R. A.; Filinchuk, Y.; Baricco, M.; Besenbacher, F.; Jensen, T. R. *J. Alloys Compd.* **2011**, *509*, 8299–8305.
- (23) Rude, L. H.; Zavorotynska, O.; Arnbjerg, L. M.; Ravnsbæk, D. B.; Malmkjær, R. A.; Grove, H.; Hauback, B. C.; Baricco, M.; Filinchuk, Y.; Besenbacher, F.; Jensen, T. R. *Int. J. Hydrogen Energy* **2011**, *36*, 15664–15672.
- (24) Ma, J.; Choudhury, N. A.; Sahai, Y. *Renewable Sustainable Energy Rev.* **2010**, *14*, 183–199.
- (25) Matsuo, M.; Nakamori, Y.; Orimo, S.; Maekawa, H.; Takamura, H. *Appl. Phys. Lett.* **2007**, *91*, 224103–224103.
- (26) Martelli, P.; Remhof, A.; Borgschulte, A.; Ackermann, R.; Strässle, T.; Embs, J. P.; Ernst, M.; Matsuo, M.; Orimo, S.-I.; Züttel, A. *J. Phys. Chem. A* **2011**, *115*, 5329–5334.
- (27) Tarascon, J. M.; Armand, M. *Nature* **2001**, *414*, 359–367.
- (28) Zhang, B. J.; Liu, B. H.; Li, Z. P. *J. Alloys Compd.* **2011**, *509*, 751–757.
- (29) Andrade-Gamboa, J.; Puzskiel, J. A.; Fernández-Albanesi, L.; Gennari, F. C. *Int. J. Hydrogen Energy* **2010**, *35*, 10324–10328.
- (30) Gennari, F. C.; Albanesi, L. F.; Puzskiel, J. A.; Larochette, P. A. *Int. J. Hydrogen Energy* **2011**, *36*, 563–570.
- (31) Sato, T.; Miwa, K.; Nakamori, Y.; Ohoyama, K.; Li, H.-W.; Noritake, T.; Aoki, M.; Towata, S.; Orimo, S. *Phys. Rev. B* **2008**, *77*, 104114–104122.
- (32) Yan, Y.; Li, H. W.; Sato, T.; Umeda, N.; Miwa, K.; Towata, S.; Orimo, S. *Int. J. Hydrogen Energy* **2009**, *34*, 5732–5736.
- (33) Jensen, T. R.; Nielsen, T. K.; Filinchuk, Y.; Jørgensen, J. E.; Cerenius, Y.; Gray, E. M.; Webb, C. J. *J. Appl. Crystallogr.* **2010**, *43*, 1456–1463.
- (34) Hammersley, A. P.; Svensson, S. O.; Hanfland, M.; Fitch, A. N.; Hausermann, D. *High Pressure Res.* **1996**, *14*, 235–248.
- (35) Vogel, S.; Ehm, L.; Knorr, K.; Braun, C. *Adv. X-Ray Anal.* **2002**, *45*, 31–33.
- (36) Boulouf, A.; Louër, D. *J. Appl. Crystallogr.* **2004**, *37*, 724–731.
- (37) PCTPro-2000 - Calorimetry and thermal analysis <http://www.setaram.com/PCTPro-2000.htm> (accessed Feb 25, 2011).
- (38) Bestpractices H2 Storage Materials www1.eere.energy.gov/hydrogenandfuelcells/pdfs/bestpractices_h2_storage_materials.pdf (accessed Apr 25, 2012).
- (39) Mak, T. C. W.; Mok, F. C. *J. Chem. Crystallogr.* **1978**, *8*, 183–191.
- (40) Maekawa, H.; Matsuo, M.; Takamura, H.; Ando, M.; Noda, Y.; Karahashi, T.; Orimo, S. *J. Am. Chem. Soc.* **2009**, *131*, 894–895.
- (41) Ravnsbæk, D. B.; Filinchuk, Y.; Černý, R.; Ley, M. B.; Haase, D.; Jakobsen, H. J.; Skibsted, J.; Jensen, T. R. *Inorg. Chem.* **2010**, *49*, 3801–3809.
- (42) Frommen, C.; Aliouane, N.; Deledda, S.; Fonnelløp, J. E.; Grove, H.; Lieutenant, K.; Llamas-Jansa, I.; Sartori, S.; Sørby, M. H.; Hauback, B. C. *J. Alloys Compd.* **2010**, *496*, 710–716.